

2023

Analytical study of lipped cold-formed steel sections with edge-stiffened hole subjected to axial compression load

Shrouck Mohammed Fouad, Mahmoud H. EL-boghdadi, Nashwa Mohamed Yossef

Follow this and additional works at: <https://digitalcommons.aaru.edu.jo/erjeng>

Recommended Citation

Mohammed Fouad, Mahmoud H. EL-boghdadi, Nashwa Mohamed Yossef, Shrouck (2023) "Analytical study of lipped cold-formed steel sections with edge-stiffened hole subjected to axial compression load," *Journal of Engineering Research*: Vol. 7: Iss. 3, Article 30.

Available at: <https://digitalcommons.aaru.edu.jo/erjeng/vol7/iss3/30>

This Article is brought to you for free and open access by Arab Journals Platform. It has been accepted for inclusion in Journal of Engineering Research by an authorized editor. The journal is hosted on [Digital Commons](#), an Elsevier platform. For more information, please contact rakan@aar.edu.jo, marah@aar.edu.jo, u.murad@aar.edu.jo.

Analytical study of lipped cold-formed steel sections with edge-stiffened hole subjected to axial compression load

Shrouk Mohammed Fouad¹, Mahmoud H. El-Boghdadi², Nashwa M. Youssef³

¹MSc Student, Structural Engineering Department, Faculty of Engineering, Tanta University – email: shourouk.foad@f-eng.tanta.edu.eg

²Professors, Structural Engineering Department, Faculty of Engineering, Tanta University – email: mahmoud.el-boghdadi@f-eng.tanta.edu.eg

³Professors, Structural Engineering Department, Faculty of Engineering, Tanta University – email: nashwa_abdeltawab@f-eng.tanta.edu.eg

Abstract- Cold-formed steel (CFS) have been widely used in different structural systems in residential and non-residential construction, especially roof structures due to many advantages. Firstly, no heat is used to form the sections unlike hot-rolled steel. Secondly, several steel thicknesses are offered to accommodate a wide range of structural and non-structural purposes. Researchers have recently searched in the usage of CFS sections, and their research showed an improvement in stiffness and strength of these sections. Therefore, the purpose of this search is to analyze and conduct the behaviour of lipped single and double channel back-to-back CFS sections with edge-stiffened hole. The built-up section attached with self-taping screws under axial compression load. The main focus of this search is to enhance comprehension of the axial behaviour of the simply supported lipped CFS channel sections by analyzing and conducting the behaviour of pinned end condition CFS columns under the effect of static displacement loading till failure and to conduct the verification of the previous finite element modelling. Additionally, this research, focus on determining how the properties of section affect the behaviour and axial strength of lipped CFS column sections and to develop the fundamental parameters and the numerical criteria needed for the non-linear analysis to model lipped CFS column sections.

Keywords: Cold-formed steel, Lipped channel sections, Axial loading tests, Finite element analysis.

I. INTRODUCTION

A research on effective design width equations for CFS columns with perforations was done in 1998 [1] to predict the ultimate strength of these members. After that a design for holes in channel CFS stub columns was developed in 2001 [2]. Methods for analyzing perforated CFS C-lipped channel columns was developed in 2005 [3]-[4] to explore distortional, local buckling, and longwave buckling, using the provisions of the direct strength method. Methods to drive the equivalent thickness of thin-walled channel CFS sections with web perforations was investigated in 2008 [5]. A numerical study was made on compression CFS members with openings in 2011 [6]. Investigations in failure modes and buckling behavior of the plates C-section with holes under compression was made in 2012 [7]. Their main aim was to describe the inelastic behavior of plates and C-section. Different compression loadings on CFS sections and the influence of various holes positions was studied in 2013 [8]. Moreover, New types of thermo-profiles with rectangular stretched perforations in C-shaped cold formed columns was studied to determine their buckling behavior in 2015 [9]. Investigations on stub columns was made in 2018 [10] to determine the ultimate strength of cold-formed rectangular [RHS] and

square [SHS] hollow sections with central circular hole at mid height. Numerical investigations was made on built-up CFS laced columns in 2020 [11]. Investigations on the built-up CFS composite action was studied in 2023 [12]. The ideal configuration for CFS built-up battened columns, consisting of two sigma (Σ) channels, was shown in the study to produce a high level of composite action. So, due to the increased manufacturing of this type of steel in recent years, CFS have been commonly used and employed as a result of their advantages as they have high strength, light weight, lack of need for a frame, rapid and easy installation, and lower handling and transportation expenses [13]. To facilitate electrical, plumbing, and heating services, among other things, many structural cold-formed steel components come with holes in various forms [14]. The location of these holes have an impact on a structural member's ultimate strength and elastic stiffness.

II. NUMERICAL MODELLING

1. General

ABAQUS software modelling program was used to conduct the behaviour of lipped single and double channel back-to-back CFS sections with slotted perforations under axial compression loading according to Chen et al. [15], [16]. The accurate determined geometric and material properties were used in the model. There are two steps involved in finite element analysis. The buckling modes (Eigen-modes) were obtained using a linear perturbation analysis (Eigen-value analysis) in the first step, and a load-displacement non-linear finite element analysis have been carried out in the next one utilizing the static procedure. Initial imperfections included in the non-linear step. Based on these finite element steps, modes of failure, load-axial shortening curves and ultimate strengths are conducted.

2. Section labels

Section labelling was used to code the depth of the web, the column's thickness, the length of the column, screw spacing, and the web hole type Figure 1. As an illustration, the label "B240-t1.75-L420-S100-NH" can be explained as:

- "B" refers to the built-up sections, "S" refers to the single ones
- "240" refers to the depth of the web, i.e. $d=240\text{mm}$

- "t1.75" refers to the thickness of the section, i.e. $t=1.75\text{mm}$
- "L420" refers to the length of the section, i.e. $L=420\text{mm}$
- "S100" refers to the spacing between the screws, i.e. $S=100\text{mm}$
- "NH" refers to the CFS section with no holes, "UH" refers to section with unstiffened holes, and "EH" refers to section with edge stiffened holes.

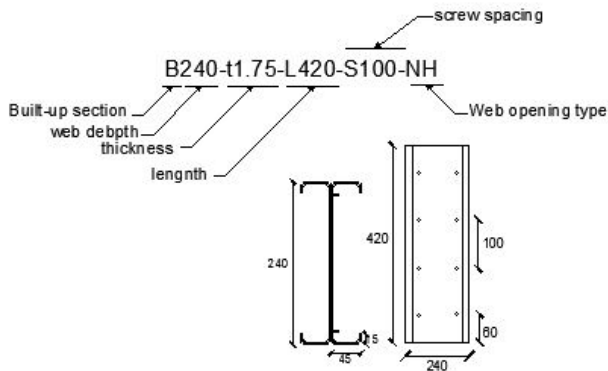


Figure 1: Section labelling illustration.

3. Finite element type and meshing

Both plain and perforated channel sections were modelled using a 4-node shell element (S4R) according to Chen et al. [15], using a mesh size of $8\text{ mm} \times 8\text{ mm}$ over the width and length, and the plates with a mesh size of $12\text{ mm} \times 12\text{ mm}$ as shown in Figure 3. According to Chen et al. [16], using a mesh size of $20\text{ mm} \times 20\text{ mm}$ over the width and length as shown in Figure 4.

It should be noted that the mesh size used in the verification model was $20\text{ mm} \times 20\text{ mm}$, while the mesh size used by Chen et al. [16] was $5\text{ mm} \times 5\text{ mm}$. Though, according to the convergence study shown in Figure 2, the mesh size $20\text{ mm} \times 20\text{ mm}$ showed a good agreement with results by Chen et al. [16].

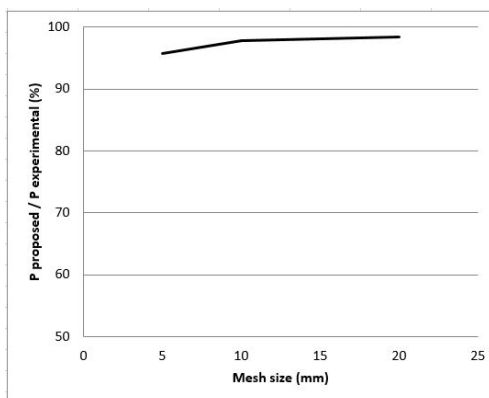


Figure 2: Convergence results with different mesh sizes for B240-t1.75-L1420-S100-EH.

4. Boundary condition and loading process

In this research, simply supported boundary conditions were used to perform the model analysis. All three translations, as well as rotation along the length of the column, were restricted for the unloaded end, whereas rotations along the vertical and horizontal moment inertia axes were allowed. Translations along the section axis were restricted for the loaded end, but rotations about the main and minor moment inertia axes, as well as longitudinal translation, were permitted as shown in Table 1. (U_x , U_y , U_z refer to three translations in axes X, Y, and Z respectively. θ_x , θ_y , θ_z refer to the rotation around the same axes. Boundary conditions illustration can be shown in Figure 5. The implicit dynamic analysis method was used in the loading process in increments according to Chen et al. [15], and general static analysis method according to Chen et al. [16]. It should be taken into consideration the simplified method as the method for performing the attached screws in the channels web according to Chen et al. [16]. So "MPC" constraint connector type was used to connect node pairs in the FE model. Load-displacement type was used to apply the loading. The contact between the built-up section was defined as node to surface type of contact pairs. The interaction was "Hard" in the normal behavior with no penetration between the two back-to-back webs. The FE model frictionless was the property used to apply the contact between the channel webs.

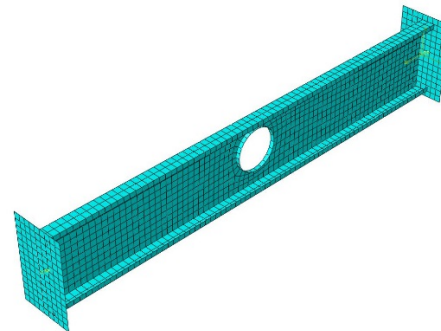


Figure 3: C240x45x15-t1.75-L1500-EH mesh.

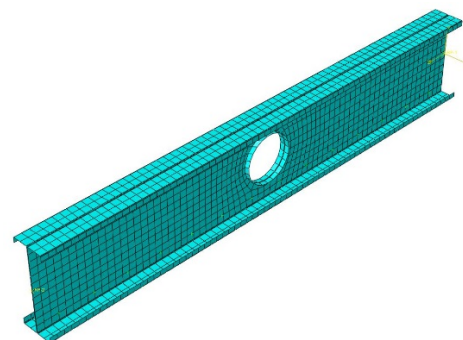


Figure 4: B240-t1.75-L1420-S100-EH mesh.

5. Section properties

The sections used in this study are "C240x45x15-t1.75-L1500-EH1", "C240x45x15-t1.75-L1500-EH3", "B240-t1.75-L920-S100-EH1", "B240-t1.75-L1420-S100-EH1", and "B240-t1.75-L1420-S50-EH1". The tensile coupon tests

from experimental study were used to add the geometric properties to the FE model including Young's modulus (E) and Poisson's ratio (ν) as mentioned in Chen et al. [15], [16]. The stress-strain curve used in the FE model is conducted from the following equations:

$$\sigma_{true} = \sigma(1 + \epsilon) \tag{1}$$

$$\epsilon_{true}(pl) = \ln(1 + \epsilon) - \frac{\sigma_{true}}{E} \tag{2}$$

Where σ_{true} is the true stress, E is the young's modulus, σ_u is the ultimate strength, ϵ and σ are the engineering strain and stress respectively. The perfect elastic plastic method was used in the model so the yield stresses are supposed to be 309.31 MPa, 317 MPa and the ultimate stresses are supposed to be 377.78 MPa, 395 MPa according to Chen et al. [15] and Chen et al. [16] in order as shown in Table 2. The hole diameter in CFS sections is 140 mm and the edge stiffener length is 13 mm.

Table 1: Boundary conditions at column ends.

Boundary conditions	U_x	U_y	U_z	θ_x	θ_y	θ_z
At roller end	1	1	0	0	0	1
At hinged end	1	1	1	0	0	1

0 \longrightarrow Free
1 \longrightarrow Restricted

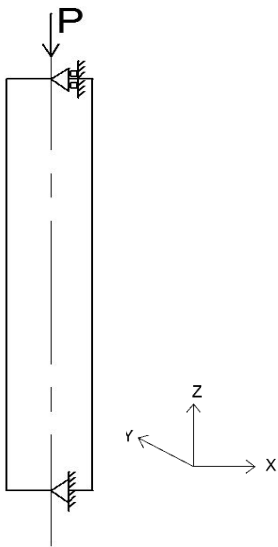


Figure 5: Boundary conditions illustration.

6. Initial imperfections

In ABAQUS, the lowest eigen mode was employed for both local and global buckling modes. For CFS single and double back-to-back channel section columns, similar modeling approaches were previously reported in the literature to represent local and overall defects. Because of restricted deformations produced throughout specimen transportation, it was discovered from the laser scanning

findings that the magnitude of local defects was more than anticipated values.

Table 2: Material properties.

Section	Yield stress (σ_y) MPa	Ultimate stress (σ_u) MPa
C240x45 x15-t1.75-L1500-EH1	309.31	377.78
C240x45 x15-t1.75-L1500-EH3	309.31	377.78
B240-t1.75-L920-S100-EH1	317.00	395.00
B240-t1.75-L1420-S100-EH1	317.00	395.00
B240-t1.75-L1420-S50-EH1	317.00	395.00

Therefore, the FEA model's validation was based on these imperfection measures. In the parametric analysis, the local buckling imperfection used in the mode is 0.5% of the channel thickness (t) according to Chen et al. [15]. This sum was calculated using information from earlier investigations. A number of FE models were used to evaluate the distortional imperfections, and it was discovered that they had little effect on the deformed shape and failure load of the columns.

III. VALIDATION PROCESS

1. Verification of lipped single and double channel back-to-back CFS sections with edge-stiffened hole

CFS sections with hinged ends were tested till failure. Sections were investigated using ABAQUS finite element analysis program till failure to conduct their behaviour according to Chen et al. [15], [16]. The validation of the section's finite element models is simulated and compared with the tested specimen conducted by Chen et al. [15], [16]. The dimensions of the cross sections in mm are shown in Figure 6. And the details of screw's spacing for back-to-back section are shown in Figure 7 according to Chen et al. [16]. Table 2 gives the yield and ultimate stresses of the specimens. The Poisson ratio, ν , was taken as 0.3.

The proposed models and the experimental results from Chen et al. [15], [16] were compared to conduct their ultimate axial strength, axial load versus axial end shortening curves, and failure modes of the sections. Local buckling for single sections failure mode was observed and distortional-overall interactive buckling was also observed for back-to-back sections. From the comparison between proposed models and experimental results, it was found that the proposed results showed a good agreement with the experimental ones.

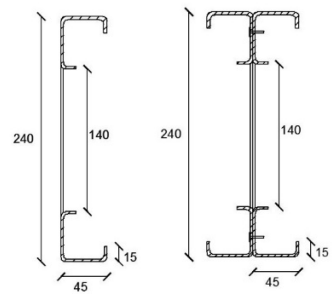


Figure 6: Cross section of specimens.

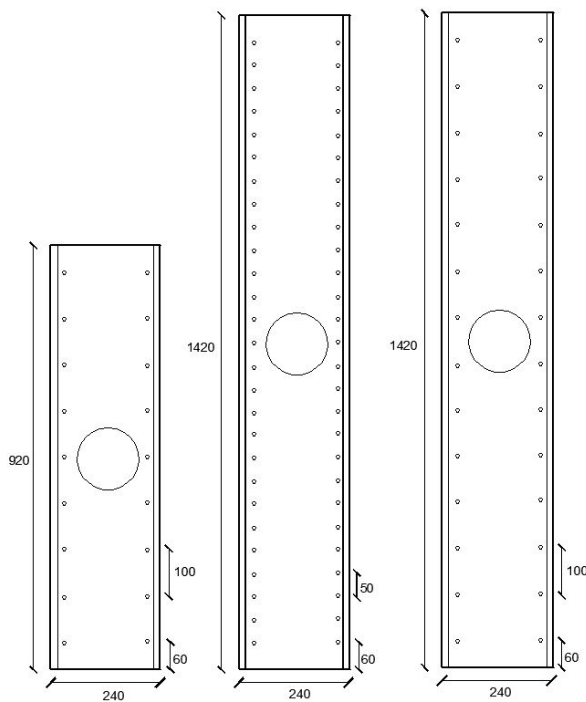


Figure 7: Screw's spacing details.

2. Test results and discussion

The experimental ultimate axial strength (P_{Exp}) with the ultimate strength from the analytical analysis modelling (P_{FEA}) recorded by Chen et al. [15], [16] and the proposed ultimate strength from our ABAQUS modelling ($P_{Proposed}$) were shown in Table 3. The experimental and numerical ultimate strength of the section "C240×45×15-t1.75-L1500-EH1" in Chen et al. [15] are 63.96 kN, and 63.52 kN respectively as shown in Table 3. Numerical result of ultimate strength in proposed ABAQUS model is 63.5 kN. This result is 0.99 of (P_{Exp}) in Chen et al. [15], so the section with edge-stiffened hole show a good agreement result with the proposed numerical result. The same was observed for section "C240×45×15-t1.75-L1500-EH3" in Chen et al. [15], the experimental and numerical ultimate strengths are 66.09 kN, and 66.78 kN respectively as shown in Table 3. The proposed ABAQUS ultimate strength result is 64.00 kN This result is 0.96 of (P_{Exp}) from Chen et al. [15], so the section also show a good agreement with the proposed numerical result. For section "B240-t1.75-L1420-S50-EH1", the experimental and numerical ultimate strengths in Chen et al. [16] are 161.1 kN and 158.3 kN, respectively as shown in Table 3. The ultimate strength of proposed ABAQUS model is 158.6 kN. This result is 0.98 of (P_{Exp}) from Chen et al. [16]. Generally, this ratio showed a good agreement to the section. The experimental and numerical ultimate strengths of the section "B240-t1.75-L1420-S100-EH1" in Chen et al. [16] are 195.2 kN, and 155.6 kN in order as shown in Table 3. Numerical result of ultimate strength in proposed ABAQUS model is 156.7 kN. This result is 0.98 of (P_{Exp}) in Chen et al. [16], so the section show a good agreement with proposed ABAQUS result. The

Doi: 10.21608/erjeng.2023.240964.1270

experimental and numerical ultimate strength of the section "B240-t1.75-L920-S100-EH1" in Chen et al. [16] are 186.3 kN, and 183.6 kN in order as shown in Table 3. Ultimate strength of proposed numerical result is 183.7 kN. This result is 0.98 of (P_{Exp}) from Chen et al. [16], so this ratio showed a good agreement with the proposed result.

Table 3: Comparison of ultimate load from experimental and FE proposed model results.

Section	Exp. Results Chen et al. [15], [16]	FEA. Results Chen et al. [15], [16]	Proposed results	Comparison
	P_{Exp} (kN)	P_{FEA} (kN)	$P_{Proposed}$ (kN)	$P_{Proposed}/P_{Exp}$
C240×45×15-t1.75-L1500-EH1	63.96	63.52	63.50	0.99
C240×45×15-t1.75-L1500-EH3	66.09	66.78	64.00	0.96
B240-t1.75-L1420-S50-EH1	161.1	158.3	158.6	0.98
B240-t1.75-L1420-S100-EH1	195.2	155.6	156.7	0.98
B240-t1.75-L920-S100-EH1	186.3	183.6	183.7	0.98

The proposed model results compared with the experimental results of Chen et al. [15], [16], showed that the proposed results reflects the behavior of the sections in Chen et al. [15], [16]. The values of ultimate strengths for Chen et al. [15], [16], the proposed ultimate strengths, and comparison ratio between them ($P_{Proposed}/P_{Exp}$), are given in Table 3.

Initially, the load versus axial shortening characteristic is linear. The columns reach the post buckling range, where non-linear behaviour predominate, when the end shortening grows and exceeds the critical buckling load. The load grows slowly in the post-buckling zone, and the stub columns fail and lose their capacity to hold further weight. As a result, when the end shortens further than the ultimate load, the load curves shrink. Comparing the proposed load versus axial load shortening curve for all sections with the experimental and numerical ones in Chen et al. [15] and Chen et al. [16], it was found a very good agreement between them. So, the study can be built based on this match as shown in Figure 8 to Figure 12.

Chen et al. [15] investigated the failure modes predicted by finite element analysis. Comparing them with the proposed ABAQUS analysis, it was found that, they were similar. Table 4, depicts the failure mode shapes for C240×45×15-t1.75-L1500-EH1, and C240×45×15-t1.75-L1500-EH3, respectively. Chen et al. [16] investigated the failure mode predicted by finite element analysis for B240-t1.75-L920-S100-EH1, B240-t1.75-L1420-S100-EH1, and B240-t1.75-L1420-S50-EH1. Comparing them with the proposed ABAQUS model, it was found that they were similar as shown in Table 5.

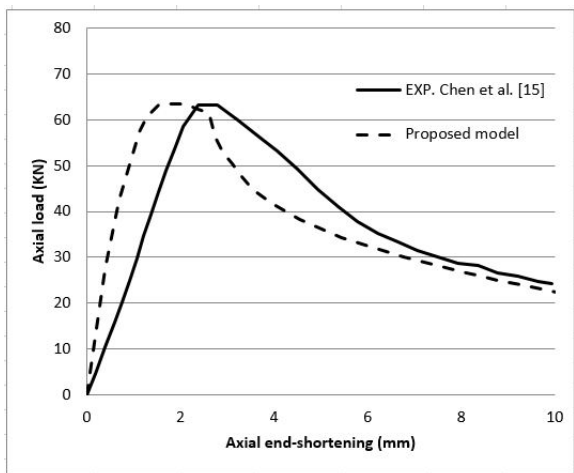


Figure 8: Axial load versus axial end-shortening for C240 x 45 x 15-L1500-EH1.

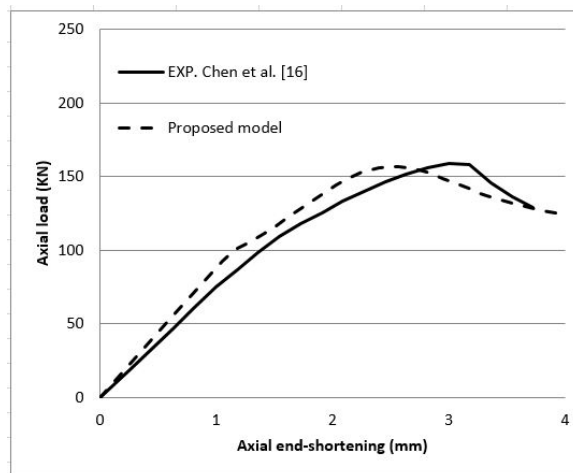


Figure 11: Axial load versus axial end-shortening for B240-t1.75-L1420-S100-EH1.

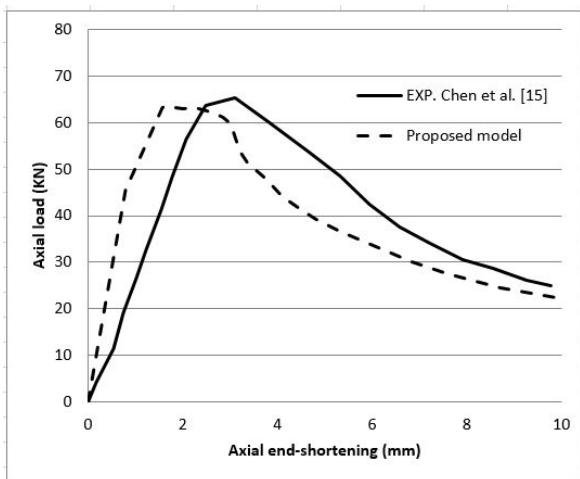


Figure 9: Axial load versus axial end-shortening for C240 x 45 x 15-L1500-EH3.

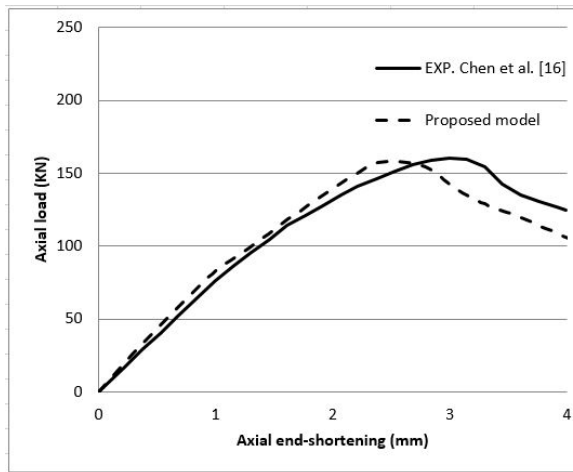


Figure 12: Axial load versus axial end-shortening for B240-t1.75-L1420-S50-EH1.

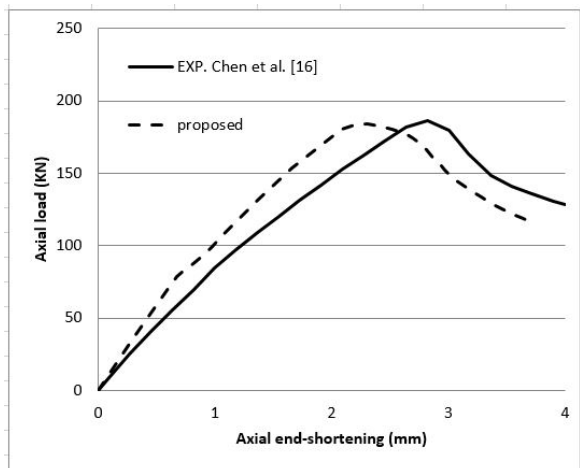


Figure 10: Axial load versus axial end-shortening for B240-t1.75-L920-S100-EH1.

Table 4: Failure modes comparison for single channels according to Chen et al. [15], and proposed validation models.

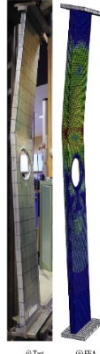
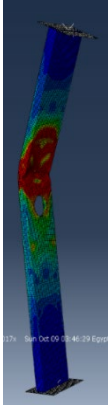

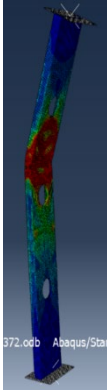
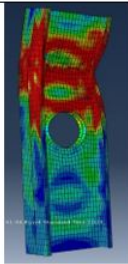
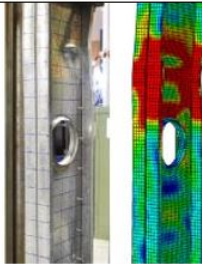
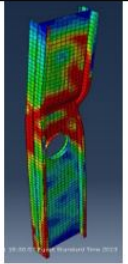

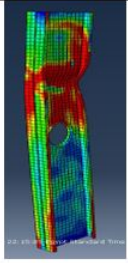
C240 × 45 × 15–L1500–EH1		C240 × 45 × 15–L1500–EH3	
Chen et al. [15] failure mode	Proposed failure mode	Chen et al. [15] failure mode	Proposed failure mode
			

Table 5: Failure mode comparison for back-to-back channels according to Chen et al. [16], and proposed validation models.

	Failure mode	
	Proposed model	Chen et al. [16] results
B240-t1.75-L920-S100-EH		
B240-t1.75-L1420-S100-EH		
B240-t1.75-L1420-S50-EH		-

IV. SUMMARY AND CONCLUSIONS

The following conclusions can be drawn from the FE modelling and validation described above:

- The finite element modelling is one of the numerical techniques that can be used to conduct solutions to a variety of engineering issues.
- To simulate the CFS single lipped channel section with edge-stiffened hole, the FE program ABAQUS was utilized. Actual measured geometric and material parameters were used in the model.
- The finite element software program ABAQUS was also used to simulate the CFS double back-to-back lipped channel section with edge-stiffened hole. The behaviour of two types of CFS sections was then conducted.
- The finite element ultimate strength results, the axial load versus axial end shortening and failure modes of the proposed ABAQUS modelling showed a good agreement with experimental and numerical results from Chen et al. [15], [16].
- According to the previous results, utilizing two channel sections as opposed to one increase considerably the column's resistance to local buckling and the section's overall effectiveness at resisting pure axial force. Comparing a single section with edge-stiffened hole with double back-to-back channel sections with edge-

stiffened hole, it was found that the efficiency at resisting pure axial load was greater for back-to-back channel sections case at the same conditions.

Funding: The authors should mention if this research has received any type of funding.

Conflicts of Interest: The authors should explicitly declare if there is a conflict of interest.

REFERENCES

- [1] N. Abdel-rahman and K. S. Sivakumaran, "Effective design width for perforated cold-formed steel compression members," 1998 NRC Canada, vol. 330, pp. 319–330, 1998.
- [2] N. E. Shanmugam and M. Dhanalakshmi, "Design for openings in cold-formed steel channel stub columns," *Thin Walled Struct.*, vol. 39, pp. 961–981, 2001.
- [3] J. Tovar and T. Sputo, "Application of direct strength method to axially loaded perforated cold-formed steel studs: Distortional and local buckling," *Thin Walled Struct.*, vol. 43, pp. 1882–1912, 2005, doi: 10.1016/j.tws.2005.08.004.
- [4] T. Sputo and J. Tovar, "Application of direct strength method to axially loaded perforated cold-formed steel studs: Longwave buckling," *Thin Walled Struct.*, vol. 43, pp. 1852–1881, 2005, doi: 10.1016/j.tws.2005.08.005.
- [5] B. Salhab and Y. C. A. Wang, "Equivalent thickness of cold-formed thin-walled channel sections with perforated webs under compression," vol. 46, pp. 823–838, 2008, doi: 10.1016/j.tws.2008.01.029.
- [6] Z. Yao, D. Ph, K. J. R. Rasmussen, and M. Asce, "Perforated Cold-Formed Steel Members in Compression. I: Parametric Studies," pp. 1–15, 2011, doi: 10.1061/(ASCE)ST.1943-541X.0001635.
- [7] Z. Yao and K. J. R. Rasmussen, "Inelastic local buckling behaviour of perforated plates and sections under compression," *Thin Walled Struct.*, vol. 61, pp. 49–70, 2012, doi: 10.1016/j.tws.2012.07.002.
- [8] M. P. Kulatunga and M. Macdonald, "Thin-Walled Structures Investigation of cold-formed steel structural members with perforations of different arrangements subjected to compression loading," *Thin Walled Struct.*, vol. 67, pp. 78–87, 2013, doi: 10.1016/j.tws.2013.02.014.
- [9] M. Garifullin, D. Trubina, and N. Vatin, "Local buckling of cold-formed steel members with edge stiffened holes," *Trans Tech Publ.*, vol. 726, pp. 697–702, 2015, doi: 10.4028/www.scientific.net/AMM.725-726.697.
- [10] T. G. Singh and K. D. Singh, "Experimental investigation on performance of perforated cold – formed steel tubular stub columns," *Thin Walled Struct.*, vol. 131, no. February, pp. 107–121, 2018, doi: 10.1016/j.tws.2018.06.042.
- [11] M. A. Sakr, S. R. El-khoriby, T. M. Khalifa, and M. T. Nagib, "International Journal of Advances in Structural and Geotechnical Engineering Special Issue for ICASGE '19 NUMERICAL MODELING OF RC SHEAR WALLS RETROFITTED WITH UHPFRC," vol. 04, no. 02, pp. 113–124, 2020.
- [12] R. Rahnavard, M. Razavi, N. Fanaie, and H. D. Craveiro, "Evaluation of the composite action of cold-formed steel built-up battened columns composed of two sigma-shaped sections," *Thin-Walled Struct.*, vol. 183, no. July 2022, p. 110390, 2023, doi: 10.1016/j.tws.2022.110390.
- [13] C. Steel, "Cold-Formed Steel in building construction," *The New Steel*, pp. 1–29, 2010.
- [14] M. Macdonald and M. P. Kulatunga, "Finite Element Analysis of Cold-Formed Steel Structural Members with Perforations Subjected to Compression Loading," *Lodz Univ. Technol.*, vol. 17, no. 2, pp. 127–139, 2013.
- [15] B. Chen, K. Roy, A. Uzzaman, G. M., D. Nash, and G. Charles Clifton, "Effects of edge-stiffened web openings on the behaviour of cold-formed steel channel sections under compression," *Thin-Walled Struct.*, vol. 144, no. July, p. 106307, 2019, doi: 10.1016/j.tws.2019.106307.
- [16] B. Chen, K. Roy, A. Uzzaman, G. Raftery, and J. B. P. Lim, "Axial strength of back-to-back cold-formed steel channels with edge-stiffened holes, un-stiffened holes and plain webs," *J. Constr. Steel Res.*, vol. 174, p. 106313, 2020, doi: 10.1016/j.jcsr.2020.106313.